

# Choroid Neovascularization Growth Prediction With Treatment Based on Reaction-Diffusion Model in 3-D OCT Images

Shuxia Zhu<sup>1</sup>, Fei Shi, Dehui Xiang, Weifang Zhu, Haoyu Chen, and Xinjian Chen, *Senior Member, IEEE*

**Abstract**—Choroid neovascularization (CNV) is caused by new blood vessels growing in the choroid and penetrating the bruch membrane. It is the major cause of vision disability in many retinal diseases. Though anti-vascular endothelial growth factor injection has proved to be effective for treating CNV, treatment planning is essential to ensure the efficacy while reducing the risk. For this purpose, we propose a CNV growth model based on longitudinal optical coherence tomography (OCT) images. The reaction-diffusion model is applied to simulate the growth and shrinkage of CNV volumes, and is solved by using the finite-element method. A fitted curve of the CNV growth/shrinkage rate is obtained by optimizing the growth parameters. Then, the trained parameters are applied to the predicted image to get the simulated image, which is compared with the validated image to evaluate the accuracy of prediction. The proposed method was tested on a dataset with seven patients in which each patient has 12 longitudinal OCT images. The resulted mean dice coefficient is  $76.40\% \pm 8.20\%$ . The experimental results show a promising step towards the image-guided patient-specific treatment.

**Index Terms**—CNV growth prediction, reaction-diffusion model, FEM.

## I. INTRODUCTION

CHOROID neovascularization (CNV) occurs when new blood vessels grow between the retina and choroid, while retina is the vision sensory area and choroid is the part of eye that contains many blood vessels. It often occurs in many serious eye diseases such as age-related macular degeneration (AMD), pathological myopia macular degeneration and histoplasmosis.

Manuscript received December 21, 2016; accepted May 1, 2017. Date of publication May 16, 2017; date of current version November 3, 2017. This study was supported in part by the National Basic Research Program of China (973 Program) under Grant 2014CB748600, in part by the National Nature Science Foundation of China for Excellent Young Scholars under Grant 61622114, in part by the National Nature Science Foundation of China under Grants 81371629, 81401472, 61401294 and 61401293, and in part by the Natural Science Foundation of Jiangsu Province under Grant BK20140052. Recommended for acceptance by D. I. I. Fotiadis. (*Corresponding author: Xinjian Chen.*)

S. Zhu, F. Shi, D. Xiang, W. Zhu, and X. Chen are with the School of Electronics and Information Engineering, Soochow University, Suzhou 215006 China (e-mail: zhushuxia01@163.com; shifei@suda.edu.cn; xiangdehui@suda.edu.cn; wfzhu@suda.edu.cn; xjchen@suda.edu.cn).

H. Chen is with the Joint Shantou International Eye Center, Shantou University and the Chinese University of Hong Kong, Shantou 515041 China (e-mail: drchenhaoyu@gmail.com).

Digital Object Identifier 10.1109/JBHI.2017.2702603

In the early stage of choroid neovascularization, there are usually no symptoms. Along with the gradual expansion of neovascular leakage and rupture, it can cause vision loss, visual distortion, or central scotoma. The patients' macula with recurrent symptoms are seriously damaged, which may cause permanent visual impairment. Choroid neovascularization can persist for months or years and then gradually become steady. It will substitute the shallow fibrovascular membrane and finally form a retinal choroidal atrophy area. The occurrence of CNV is highly related to the high concentration of vascular endothelial growth factors (VEGF) [1].

Currently, the most effective medical treatment for CNV is intravitreal injection of anti-VEGF medicine. This treatment can inhibit the growth of CNV and reduce the area of fluid below the retinal pigment epithelium (RPE). However, it requires frequent injections, which may cause complications that can result in impairment of sight or complete loss of vision. Moreover, this treatment is very expensive and it may have little curative effect for specific patients [2].

Optical coherence tomography (OCT) was first proposed in 1991 by Huang *et al.* [3]. OCT is a non-invasion and non-contact imaging modality. It provides 3D reconstructional images of biological tissues with a high longitudinal resolution. From the retinal OCT images, we can quantitatively measure the size, position and shape of changeable lesion area, and in this way, tracking disease condition can be achieved. OCT imaging as a rapid imaging modality, three-dimensional information and subtle changes over time can reflect the disease, so it is the most effective tool for monitoring the condition of CNV. In [4], OCT has been used to design the treatment plan preliminary. In the PrONTO (Prospective OCT Imaging of Patients with Neovascular AMD Treated with Intra-Ocular Lucentis) trial, patients are given three injections of ranibizumab at one month intervals, where the dosing regimen is variable, whereafter patients were only re-injected based on specific criteria. Retinal OCT images can provide clinically useful information for the diagnosis of diseases of the optic nerve head and central fovea, such as CNV, glaucoma, AMD and so on [5], [6]. OCT is useful in quantitatively evaluating cystoid edema, intraretinal and sub-retinal fluid and in monitoring CNV before and after intravitreal injection [7]. Fig. 1 shows an example of retinal OCT image with CNV.

There are several previous works focusing on quantitative analysis of CNV. Bogunovic *et al.* [8] predicted the outcome

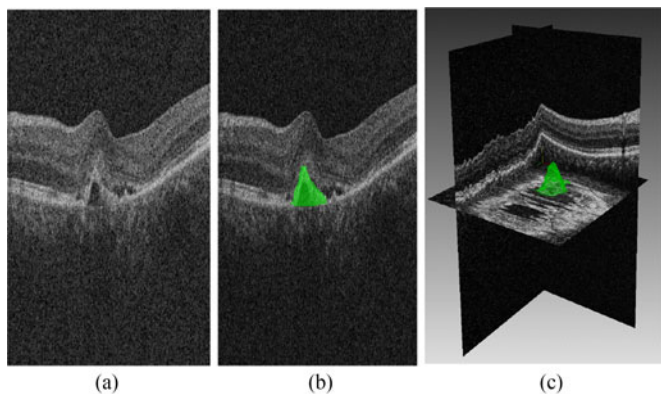


Fig. 1. An example of retinal OCT image with CNV in green color. (a) A B-scan of the original retinal OCT image; (b) CNV ground truth shown in green; (c) 3D visualization.

of the induction phase using statistical quantitative analysis. However they just predicted the responder or non-responder to the treatment and did not point out the future status of disease regions. Xu *et al.* [9] delineated 3D artificial vascular network. In [10], Wolf-Dieter *et al.* selected features to predict the retinal disease recurrence under treatment. But their methods are not intend to predict the CNV growth accurately and all based on qualitative analysis and simple indicators.

In this paper, we propose a CNV growth model for longitudinal OCT images through mathematical modeling: reaction diffusion model, and finite element method (FEM) is used to solve the equation in the reaction-diffusion model. Optimal growth parameters can be obtained by minimizing an objective function of overlap accuracy, and genetic algorithms is applied in this objective function. The proposed method is tested on a dataset with 7 patients each has 12 OCT images and the experimental results show the accuracy of the proposed method. A preliminary version of this work has been published in Zhu *et al.* (2016) [11]. We extend the previous work by a more reasonable model, providing more experimental data and detailed analysis of results. In addition, we conduct several additional experiments, including a more robust pre-processing method to ensure the prediction accuracy, prediction performance at different time points, and visualization of comparison of results and ground truth.

## II. METHOD

### A. Method Overview

The framework of our method is shown in Fig. 2. Suppose there are  $N$  images in the longitudinal study and the first  $N-1$  images are used for training the growth parameters to predict the remaining  $N$ -th image. Firstly, image preprocessing is conducted on these OCT images. Secondly, tetrahedral meshes are constructed for the segmented CNV volumes and surrounding tissues. Thirdly, the CNV growth model is applied on the first  $N-1$  images to get the optimal parameters. Then curve fitting is applied on these estimated parameters to predict the parameter for the  $N$ -th image. In the end, the predicted image is compared with the true  $N$ -th image to evaluate the accuracy.

### B. Data Acquisition

3D OCT images with  $512 \times 1024 \times 128$  voxels ( $11.72 \mu\text{m} \times 5.86 \mu\text{m} \times 15.6 \mu\text{m}$ ), covering the volume of  $6 \text{ mm} \times 6 \text{ mm} \times 2 \text{ mm}$ , are obtained by ZEISS scanner. These images are acquired once a month from 7 patients during a 12-month clinical trial. In this trial, patients are classified into treatment group (4 patients) or reference group (3 patients) randomly, and they are represented in T1, T2, T3, T4, R1, R2 and R3. The treatment plan includes two phases: core treatment phase and extended treatment phase. In the first phase, patients in treatment group are given three intravitreal anti-VEGF injections (conbercept, 0.5 mg) at one month interval (month 0, 1, 2), while patients in reference group are injected with condolences agent. In the end of third month, a periodic assessment is performed. In the second phase, patients in treatment group are injected medicine at three month intervals, while in the first three months of this phase, patients in reference group are injected medicine every month, then medicine are injected at three month intervals. In the end of 12th month, a final assessment is performed. The treatment plans of treatment group and reference group are shown in Fig. 3.

### C. Preprocessing

Image registration is first conducted on the OCT images. In this longitudinal study, the images are collected from different times. Displacement of the retina in OCT images are often caused by different position of the eye during scanning. The displacements severely affect the final prediction accuracy. Hence, in order to observe the change of lesion area at the same positions and guarantee prediction accuracy, images registration is necessary for us. In the paper, the first image is used as the reference image and other images are registered to it via a rigid transformation based on manually input landmarks [12]. One example of the registration results can be seen in Fig. 4.

Secondly, a segmentation is performed to CNV based on graph cut. CNV segmentation is a very important step, because segmentation results directly affect the accuracy of prediction results. Surface segmentation is first conducted based on a graph-search method [13], and the surface segmentation results are used to localize the CNV regions [14]. We use this method to segment the surface 1, 2, 3 and 4 corresponding to the upper boundary of nerve fiber layer (NFL), the boundary between outer plexiform layer (OPL) and outer nuclear layer (ONL), the boundary between verhoeff's membrane (VM) and retinal pigment epithelium (RPE) and bruch membrane (BM). For the data with poor segmentation results, we modified the local segmentation results manually under the guidance of an experienced ophthalmologist. Because the lower boundary of the choroid is difficult to identify, and it is approximated by a surface with a fixed distance to surface 4. One segmentation result is shown in Fig. 5.

### D. Meshing

Meshing is an important step in modeling based on finite element method. The overall structure of the grid from top to

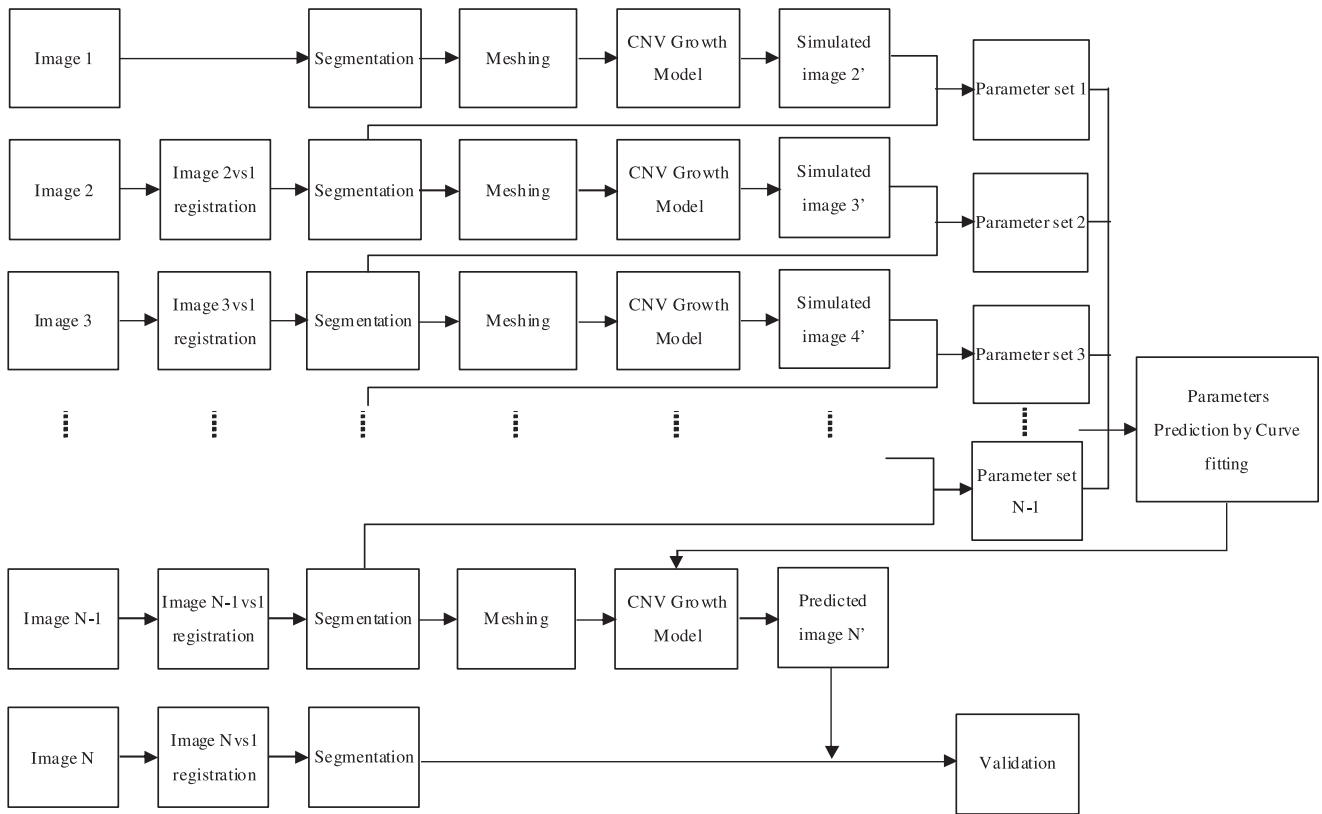


Fig. 2. Framework of the proposed method.

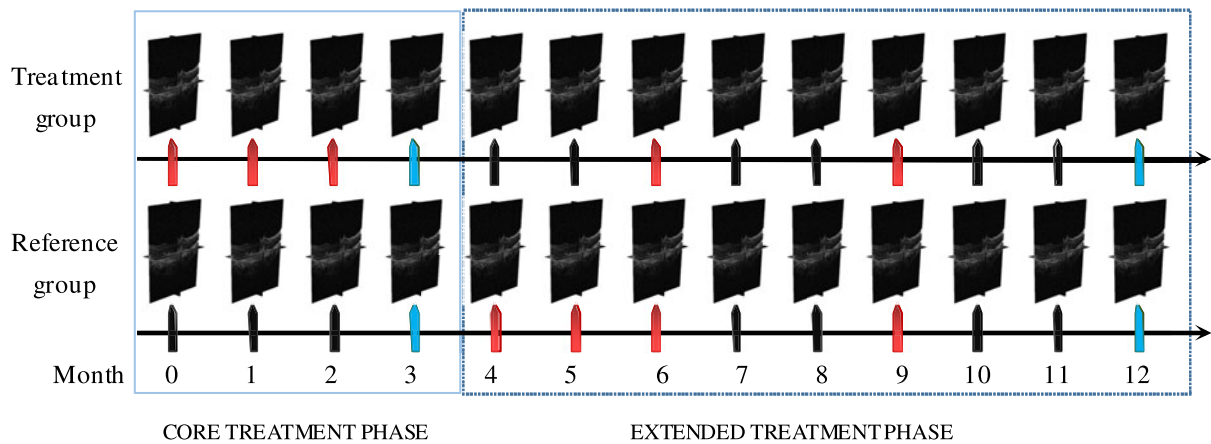


Fig. 3. Illustration of the injection on treatment group and reference group. The red arrows represent treatment of intravitreal injections, the black arrows represent the injection of condolences agent and the blue arrows represent the assessment time.

bottom are Mesh, Element, Node and Voxel. The relationships between the Mesh, Element, Node and Voxel are shown in Fig. 6. In Fig. 6, the Element structure is a tetrahedral structure. Voxel is the basic unit in the image, the entire image is composed of voxels, and the voxel is also the basic unit of the entire mesh.

For the aim of creating mesh, firstly, we need to break the entire image into node, then 4 nodes can form an element. The size of node can be set freely. In this paper, each node consists of an average of 12 (3×2×2) voxels. In fact, the size of node can be adjusted, if a node contains more number of voxels, the

more sparse is the image divided. So the amount of calculation will become smaller, but the accuracy will also be decreased. On the contrary, if a node contains fewer voxels, the prediction accuracy will be increased, but the amount of calculation will become much more.

In this paper, Tetrahedral meshing is conducted on the segmented CNV volumes and retinal layers using ISO2Mesh method [15], which is a 3D surface and volumetric mesh generator. It includes a number of free mesh processing utilities and can produce high quality 3D tetrahedral mesh or triangular

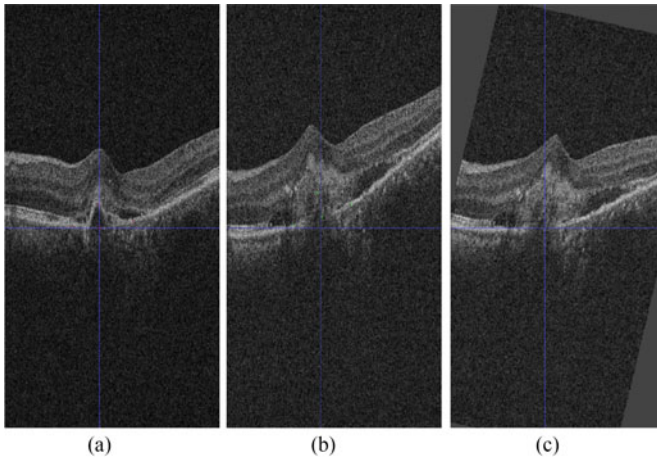


Fig. 4. Example of registration. (a) Fixed image; (b) Moving image; (c) Registration result.

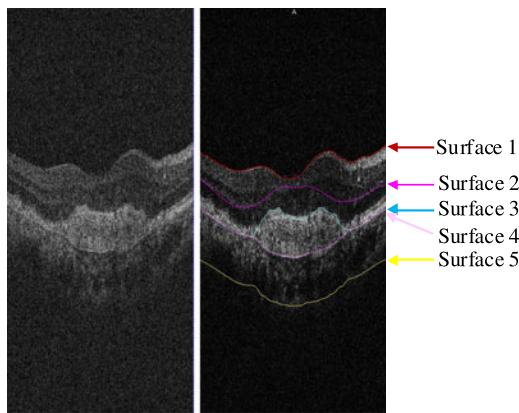


Fig. 5. Example of layer segmentation. (a) Original OCT image; (b) Surface segmentation result with local modification.

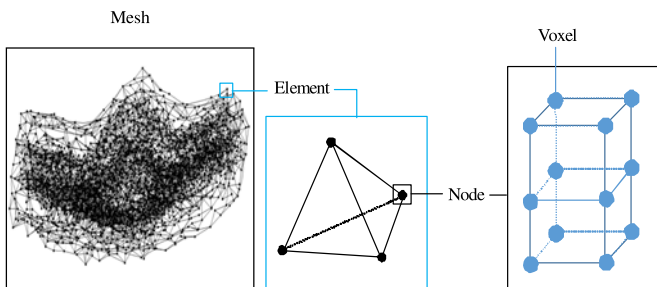


Fig. 6. A schematic diagram of meshing in retinal images.

surface directly from segmented, binary or grayscale medical images [16].

Meshing procedure includes the following two steps:

- 1) Triangular iso-surfaces with the specified density are generated for the input segmented 3D retinal OCT image.
- 2) Tetrahedral elements are filled for the sub-volumes, which are bounded by the previously generated iso-surfaces. Sub-regional labels can be supplied so that the resulted FEM mesh can carry sub-domains that

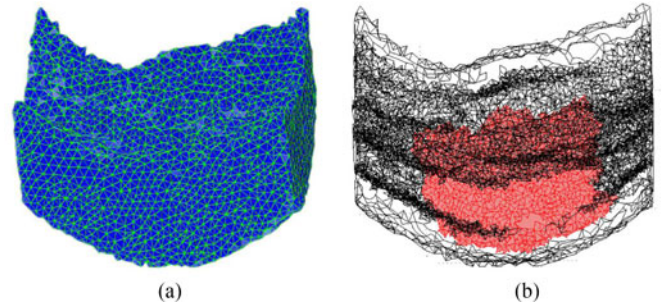


Fig. 7. The meshing retinal OCT image. (a) The meshing surface; (b) The meshing CNV region in red colour.

correspond to different tissue types (CNV volumes and retinal layers).

One result of retinal volumetric mesh generation is given in Fig. 7.

### E. CNV Growth Model

The reaction-diffusion model [17] is a mathematical model which is widely used in geology, biology and physics. It describes the substances distributed in space and temporal development. In [18]–[20], reaction-diffusion models were used to model the tumor growth, but in these models, the effect of treatment was not considered. In this paper, the model is first applied to simulate both the invasion of CNV without treatment and the shrink of CNV under the treatment. It is worth noting that we design the treatment term to represent the effect of medicine. The model can be defined as follows:

$$\frac{\partial u}{\partial t} = f(u, t) + \nabla \cdot (c \nabla u) - a \cdot u \quad (1)$$

where  $u$  represents the dimensionless concentration of CNV with the initial value of 4000.  $c$  stands for diffusion coefficient of CNV volumes towards surrounding tissues, and  $a \cdot u$  is the treatment term, where  $a$  is set to a constant.

The source function  $f$  can be formulated using Logistic model [21], which is a popular technique for the prediction of numeric values. It is defined as follows:

$$f(u, t) = \rho \cdot u(1 - u) \quad (2)$$

where  $\rho$  is the growth rate of CNV. Combining (1) and (2), we can get

$$\frac{\partial u}{\partial t} = \rho \cdot u(1 - u) + \nabla \cdot (c \nabla u) - a \cdot u \quad (3)$$

$$c \nabla u \cdot \vec{n}_{\partial \Omega} = 0 \quad (4)$$

Equation (4) enforces Neumann boundary conditions on the retinal domain  $\Omega$ . Then, we apply the finite element method [22], [23] to solve the partial differential equations in the above reaction-diffusion model. Therefore, based on the Galerkin method [24], the continuous problem can be converted to a discrete problem in a subvectorial space of finite dimension.

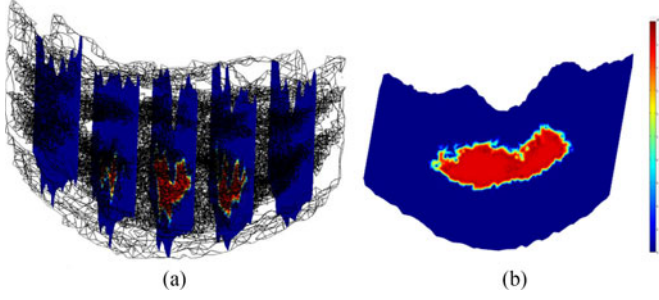


Fig. 8. Two examples of the modeling result. (a) is simulated CNV density; (b) is a slice of simulated image.

The modeling results can be seen in Fig. 8, we segment the modeling result with the threshold value of 4000 to get the simulated image  $\hat{I}_{i+1}$ .

### F. Growth Parameters Training

In our CNV growth model, the parameters  $\rho$  and  $c$  are needed to be estimated. For a particular patient, the optimal set of CNV growth parameters is not known. We assume  $c$  is a constant over time, while the value of  $\rho$  varies with time which can be estimated from the longitudinal OCT images.

$$\theta^* = \arg \min_{\theta} E(\theta) \quad (5)$$

To get the optimal value of  $\theta^*$ , we minimize the following objective function  $E(\theta)$  of overlap accuracy [25].

$$E(\theta) = \sum_{i=1}^{11} w \cdot (1 - TPVF(\hat{I}_{i+1}(\theta), I_{i+1})) + (1 - w) \cdot FPVF(\hat{I}_{i+1}(\theta), I_{i+1}). \quad (6)$$

$$TPVF = \frac{|\hat{I}_{i+1} \cap I_{i+1}|}{|I_{i+1}|} \quad (7)$$

$$FPVF = \frac{|\hat{I}_{i+1} - |\hat{I}_{i+1} \cap I_{i+1}|}{|I_{\Omega}| - |I_{i+1}|} \quad (8)$$

where  $\theta = \{\rho_1, \rho_2, \dots, \rho_{11}; c\}$ ,  $|\ast|$  represents the volume of  $\ast$ ,  $\hat{I}_{i+1}$  is the simulated CNV area achieved from the true  $i$ th images,  $I_{i+1}$  is the true CNV area in  $i + 1$ th image and  $I_{\Omega}$  is the region of interest in retinal OCT image. The true positive volume fraction (TPVF) represents the proportion of truly identified CNV volume in the true CNV volume and the false positive volume fraction (FPVF) denotes the proportion of falsely predicted CNV volume in the total background volume.  $w$  is set to 0.5 in this paper for equal weight of true positive and false positive. In order to optimize the parameters  $\theta^*$ , genetic algorithms [26] is applied in this objective function. The algorithm has low time complexity and high efficiency. Because selection of the initial parameter in the algorithm is random, so each calculation results may be different, we run the algorithm several times and analysis the results. After we exclude the outliers, the average value of the remaining results is taken as the optimal parameter.

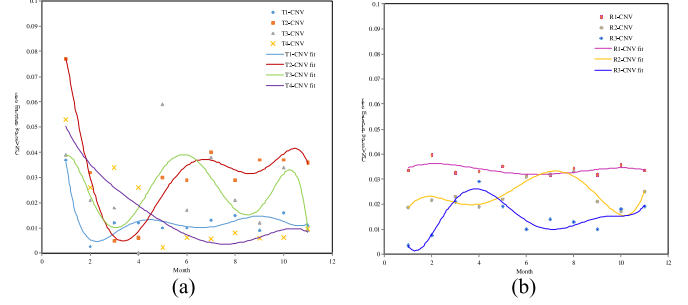


Fig. 9. (a) and (b) represent CNV growth parameters curve of treatment group and reference group.

TABLE I  
TPVF, FPVF AND DICE OF THE PREDICTION WITH GROUND TRUTH I IN MONTH 12

	TPVF(%)	FPVF(%)	DICE(%)
Patient T1	83.54	3.52	76.72
Patient T2	75.56	3.72	72.02
Patient T3	74.67	3.56	80.85
Patient T4	87.58	1.89	84.91
Patient R1	79.51	2.89	80.24
Patient R2	82.40	1.41	83.56
Patient R3	65.63	0.12	76.24

In our experiment, the dataset of real case OCT with resolution  $512 \times 1024 \times 128$  is used. The time period between two scans is one month and there are 84 ( $12 \times 7$ ) OCT images in total. For each patient, the first 11 images are used for training. They are all applied to the reaction-diffusion model to compute the prediction result for the 12th image. Then the result is validated by comparing it with the real 12th image. Fig. 9 shows the curves of the fitted CNV growth parameters for the 7 patients.

### III. EXPERIMENTAL RESULTS

Two experts manually and independently segmented the CNV areas in each B-scan and the results are used as ground truth to evaluate the accuracy of prediction. The correlation of CNV volumes of ground truth I, ground truth II and the predicted results are shown in Fig. 10. From the figure, we can know that the predicted results and these two ground truth are highly positively correlated. Besides, ground truth I and ground truth II are also positively correlated. The correlation coefficient calculation formula is shown in (9).  $v$  is the ground truth and  $\hat{v}$  is the predicted CNV volumes. The correlation coefficients are 0.988, 0.993 and 0.978 respectively. So we choose one ground truth randomly for comparison. The results of CNV growth prediction can be seen in Fig. 11. It shows the manually segmented CNV results from ground truth I by overlaid on the original images and the red lines shows the prediction results. The TPVF, FPVF and DICE of prediction results are presented in Table I. The dice index indicates similarity between the real CNV volume and predicted CNV volume and is used here to evaluate the overall performance of the proposed method. The mean dice

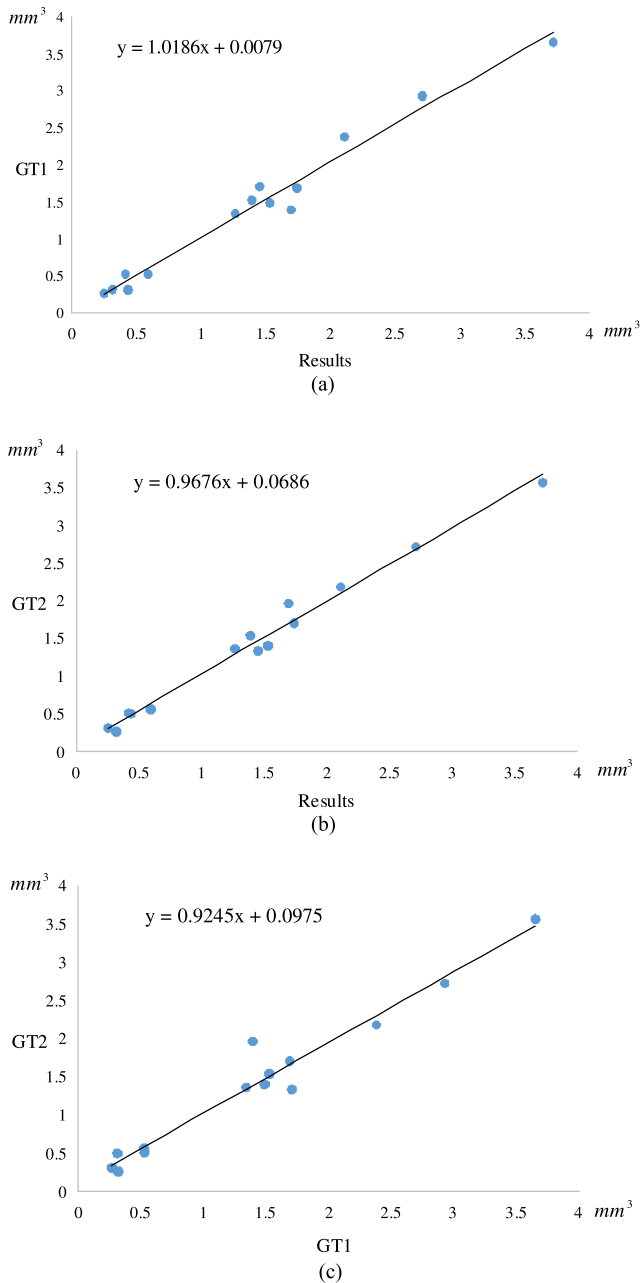


Fig. 10. (a), (b) and (c) represent the correlation of ground truth I with the predicted results, the correlation of ground truth II with the predicted results and the correlation of ground truth I with ground truth II, respectively.

coefficient is 78.41%, which shows the efficacy of the proposed method to predict the future status of CNV volumes.

In addition, we also evaluate the performance of this model in month 3, month 6 and month 9, and the prediction results can be seen in Table II, Table III and Table IV. The mean dice is 77.21%, 71.31% and 73.08%, respectively. The results show that the proposed method has high stability in multi-time point prediction. It can be seen in Table III, the dice coefficient of T2 and T3 are low, it may partly due to the complications, such as subretinal fluid (SRF), pigment epithelial detachment (PED) and cystoid edema. These complications lead to uncertainty about

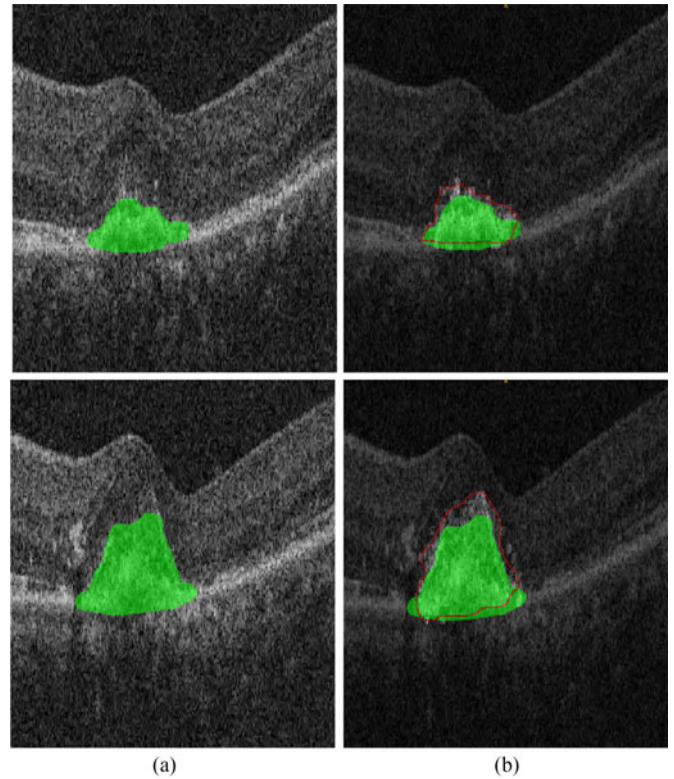


Fig. 11. Two examples of CNV growth prediction results. (a) OCT images with the CNV segmented in green; (b) Comparison between the clinical segmentation and the prediction.

TABLE II  
TPVF, FPVF AND DICE OF THE PREDICTION WITH GROUND TRUTH I IN MONTH 3

	TPVF(%)	FPVF(%)	DICE(%)
Patient T1	71.37	2.01	70.87
Patient T2	68.75	1.59	75.40
Patient T3	71.05	2.74	71.96
Patient T4	87.38	3.18	84.46
Patient R1	79.57	0.41	84.14
Patient R2	87.00	2.98	81.70
Patient R3	75.32	0.30	84.49

CNV growth.

$$r = \frac{\sum_{i=1}^n (\hat{v}_i - \bar{\hat{v}})(v_i - \bar{v}_i)}{\sqrt{\sum_{i=1}^n (\hat{v}_i - \bar{\hat{v}})^2} \cdot \sqrt{\sum_{i=1}^n (v_i - \bar{v}_i)^2}} \quad (9)$$

#### IV. DISCUSSION

We have proposed a method to predict the CNV growth with treatment based on reaction diffusion model in 3D OCT images. Experimental results show the accuracy and feasibility of the method. However, our method has two limitations. First, the experimental population size (7 patients) is small. This mainly due to the high cost of medicine and patients are hard to follow a long and strict treatment planning. Second, the segmentation of OCT images with such disease is a difficult task, the

**TABLE III**

TPVF, FPVF AND DICE OF THE PREDICTION WITH GROUND TRUTH I IN MONTH 6

	TPVF(%)	FPVF(%)	DICE(%)
Patient T1	75.00	1.77	76.40
Patient T2	63.07	1.90	69.25
Patient T3	51.50	3.31	53.17
Patient T4	86.32	1.88	88.05
Patient R1	75.87	1.21	80.68
Patient R2	72.84	1.73	78.68
Patient R3	74.57	1.53	72.27

**TABLE IV**

TPVF, FPVF AND DICE OF THE PREDICTION WITH GROUND TRUTH I IN MONTH 9

	TPVF(%)	FPVF(%)	DICE(%)
Patient T1	82.61	1.60	80.98
Patient T2	66.19	2.94	70.93
Patient T3	76.32	4.18	67.77
Patient T4	83.36	2.44	83.38
Patient R1	60.30	2.84	64.13
Patient R2	77.85	0.85	84.16
Patient R3	64.90	3.01	61.84

method in our paper does not perform well for a few cases. As a result, the prediction results are affected by the segmentation errors.

In the future, we will investigate the optimal dosing treatment and injection time interval for personalization. Finally, we believe that such a method could help the clinical patient-specific treatment planning.

## V. CONCLUSION

In this paper, we present a method to predict the CNV status in the future time under treatment from a longitudinal study. To the best of our knowledge, this is the first attempt to predict CNV growth. The proposed method is tested on a dataset with 84 longitudinal OCT images and these images are collected from 7 patients who suffering with choroidal neovascular. The mean TPVF, FPVF and DICE are 75.00%, 2.19% and 76.40%, respectively. The linear regression analysis of the predicted results and the manually segmented ground truth show that they have a strong correlation. The results are promising in achieving the size and location of the future CNV region. It also can be used to guide the treatment planning in clinical practice. In the end of core treatment phase, periodic assessment is done. Fig. 12 shows the measurements at the first three months. In treatment group, anti-VEGF medicine are injected, and the disease area are decrease obviously, while in the reference group, the disease become worse or not shrinked. We can know that anti-VEGF medicine can inhibit the growth of blood vessels and prevent disease progression effectively.

In the end of extended phase, we do a final assessment. CNV growth parameter is the important factor for prediction.

From the Fig. 9, we can see that the therapeutic effects are obvious after the injection in the treatment group. The condition of patients T1 and T4 become stable, but the disease of patients

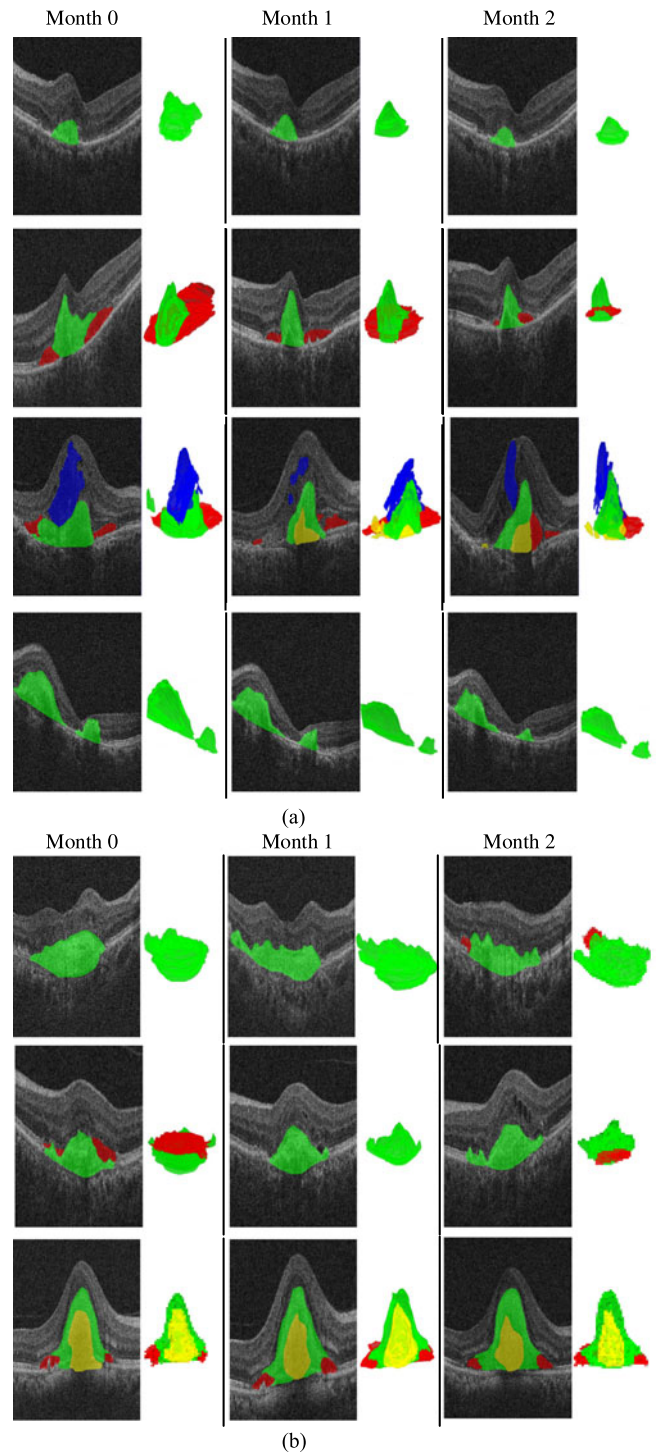
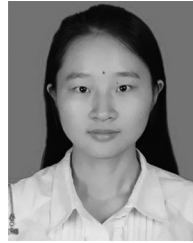


Fig. 12. Measurements at first three months. (a) 4 patients in treatment group with segmented disease area; (b) 3 patients in reference group with segmented disease area; Green, red, yellow and blue in a Bscan and 3D visualization represent CNV area, subretinal fluid (SRF), pigment epithelial detachment (PED) and cystoid edema.

T2 and T3 recurrent frequently. According to the results of prediction, ophthalmologist could make different treatment plans based on the patients' response to medicine. In reference group, patient R1 has no response to the medicine and patient R2 has little response to the treatment, which is the representative of a few population.

## REFERENCES

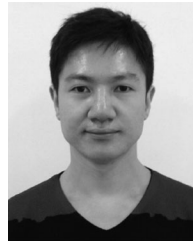
- [1] N. Kwak *et al.*, "VEGF is major stimulator in model of choroidal neovascularization," *Investigative Ophthalmol. Visual Sci.*, vol. 41, no. 10, pp. 3158–3164, 2000.
- [2] A. Kubicka-Trzaska *et al.*, "Circulating anti-retinal antibodies predict the outcome of anti-VEGF therapy in patients with exudative age-related macular degeneration," *Acta Ophthalmologica*, vol. 90, no. 1, pp. 21–24, 2012.
- [3] D. Huang *et al.*, "Optical coherence tomography," *Science*, vol. 254, no. 5035, pp. 1178–1181, 1991.
- [4] P. J. Rosenfeld *et al.*, "Visual acuity outcomes following a variable-dosing regimen for ranibizumab (lucentis™) in neovascular AMD: The PrONTO study," *Invest. Ophthalmol. Vis. Sci.*, vol. 47, no.13, pp. 2958, 2006.
- [5] W. Drexler and J. G. Fujimoto, "State-of-the-art retinal optical coherence tomography," *Prog. Retinal Eye Res.*, vol. 27, no. 1, pp. 45–88, 2008.
- [6] G. J. Jaffe and J. Caprioli, "Optical coherence tomography to detect and manage retinal disease and glaucoma," *Amer. J. Ophthalmol.*, vol. 137, no. 1, pp. 156–69, 2004.
- [7] M. R. Hee *et al.*, "Optical coherence tomography of age-related macular degeneration and choroidal neovascularization," *Ophthalmology*, vol. 103, no. 8, pp. 1260–1270, 1996.
- [8] H. Bogunovic, D. Michael, L. Z. Abramoff, and M. Sonka, "Prediction of treatment response from retinal OCT in patients with exudative age-related macular degeneration," *IEEE Int. Conf. Unmanned Aircraft Syst.*, pp. 524–533, 2014.
- [9] T. Xu *et al.*, "Delineating 3D angiogenic sprouting in OCT images via multiple active contours," in *Augmented Reality Environments for Medical Imaging and Computer-Assisted Interventions*. Berlin, Germany: Springer, 2013, pp. 231–240.
- [10] W.-D. Vogl *et al.*, "Spatio-temporal signatures to predict retinal disease recurrence," in *Proc. Int. Conf. Inf. Process. Med. Imag.*, 2015, vol. 24, pp. 152–163.
- [11] S. Zhu *et al.*, "3D choroid neovascularization growth prediction based on reaction-diffusion model," *SPIE*, vol. 9788, 2016, Art. no. 978807.
- [12] X. Guo, "Three-dimensional moment invariants under rigid transformation," *Lect. Notes Comput. Sci.*, vol. 719, pp. 518–522, 1993.
- [13] F. Shi *et al.*, "Automated 3-D retinal layer segmentation of macular optical coherence tomography images with serous pigment epithelial detachments," *IEEE Trans. Med. Imag.*, vol. 34, no. 2, pp. 441–452, Feb. 2015.
- [14] X. Chen, M. Niemeijer, L. Zhang, K. Lee, M. D. Abramoff, and M. Sonka, "Three-dimensional segmentation of fluid-associated abnormalities in retinal OCT: Probability constrained graph-search-graph-cut," *IEEE Trans. Med. Imag.*, vol. 31, no. 8, pp. 1521–1531, Aug. 2012.
- [15] Q. Fang. (2010). ISO2Mesh: A 3D surface and volumetric mesh generator for MATLAB/octave. [Online]. Available: <http://iso2mesh.sourceforge.net/cgi-bin/index.cgi?Hom>
- [16] Q. Fang and D. A. Boas, "Tetrahedral mesh generation from volumetric binary and grayscale images," in *Proc. 6th IEEE Int. Conf. Symp. Biomed. Imag., Nano Macro*, 2009, pp. 1142–1145.
- [17] A. E. Islam *et al.*, "Reaction-diffusion model," *Springer Ser. Adv. Microelectron.*, vol. 139, pp. 181–207, 2016.
- [18] X. Chen, R. M. Summers, and J. Yao, "Kidney tumor growth prediction by coupling reaction-diffusion and biomechanical model," *IEEE Trans. Biomed. Eng.*, vol. 60, no. 1, pp. 169–173, Jan. 2013.
- [19] K. C. L. Wong *et al.*, "Pancreatic tumor growth prediction with multiplicative growth and image-derived motion," *Inf. Process. Med. Imag.*, vol. 24, pp. 501–513, 2015.
- [20] M. Lê *et al.*, "Bayesian personalization of brain tumor growth model," in *Medical Image Computing and Computer-Assisted Intervention*. New York, NY, USA: Springer, 2015, pp. 424–432.
- [21] J. Friedman, T. Hastie, and R. Tibshirani, "Additive logistic regression: A statistical view of boosting," *Ann. Stat.*, vol. 28, no. 2, pp. 337–407, 2000.
- [22] K.-J. Bathe, *Finite Element Method*. London, U.K.: Butterworth-Heinemann, 2000, pp. 394–409.
- [23] A. Mohamed and C. Davatzikos, "Finite element modeling of brain tumor mass-effect from 3D medical images," *Med. Image Comput. Comput.-Assist. Intervention*, vol. 8, pp. 400–408, 2005.
- [24] A. I. Hanhart, M. K. Gobbert, and L. T. Izu, "A memory-efficient finite element method for systems of reaction-diffusion equations with nonsmooth forcing," *J. Comput. Appl. Math.*, vol. 169, no. 2, pp. 431–458, 2010.
- [25] C. Hoge, C. Davatzikos, and G. Biros, "An image-driven parameter estimation problem for a reaction-diffusion glioma growth model with mass effects," *J. Math. Biol.*, vol. 56, no. 6, pp. 793–825, 2008.
- [26] S. Austin, "An introduction to genetic algorithms," *Quart. Rev. Biol.*, vol. 24, nos. 4/5, pp. 325–336, 1996.



**Shuxia Zhu** received the Master's degree in electronics and information engineering from Soochow University, China, in 2017. Her current research interests include medical data segmentation, medical image analysis, and mathematical modeling.



**Fei Shi** received the Ph.D. degree in electrical engineering from Polytechnic University (now New York University Tandon School of Engineering), Brooklyn, NY, USA, in 2006. She is currently an Assistant Professor at Soochow University, Suzhou, China. She has coauthored more than 20 papers in internationally recognized journals and conferences. Her current research is focused on medical image processing and analysis.



**Deihui Xiang** received the B.E. degree in automation from Sichuan University, Sichuan, China, in 2007, and the Ph.D. degree from the Institute of Automation, Chinese Academy of Sciences, Beijing, China, in 2012. He is currently an Associate Professor with the School of Electronics and Information Engineering, Soochow University, Jiangsu, China. His current research interests include medical image analysis, computer vision, medical data visualization, and pattern recognition.



**Weifang Zhu** received the Ph.D. degree in electrical engineering from Soochow University, Suzhou, China, in 2013. She is currently an Associate Professor at Soochow University. She has coauthored more than 15 papers in internationally recognized journals and conferences. Her current research is focused on medical image processing and analysis.



**Xinjian Chen** (SM'15) received the Ph.D. degree from the Institute of Automation, Chinese Academy of Sciences, Beijing, China, in 2006. After graduation, he worked on research projects with several prestigious groups: Microsoft Research Asia, Beijing, China (2006–2007); Medical Image Processing Group, University of Pennsylvania (2008–2009); the Department of Radiology and Image Sciences, National Institutes of Health (2009–2011); and the Department of Electrical and Computer Engineering, University of Iowa (2011–2012). In 2012, he joined the School of Electrical and Information Engineering, Soochow University, Suzhou, China, where he is a Distinguished Professor and the Director of Medical Image Processing, Analysis and Visualization Laboratory. He is currently an Associate Editor of the IEEE TRANSACTIONS ON MEDICAL IMAGING and the IEEE JOURNAL OF TRANSLATIONAL ENGINEERING IN HEALTH AND MEDICINE. Until now, he has published more than 100 peer-reviewed papers in prestigious international journals and conferences, and holds 6 granted patents and 20 pending status patents. His research interests include medical image processing, image analysis, pattern recognition, artificial intelligence, etc.